Morphology and optical properties of CeF_3 and CeF_3:Tb nanocrystals: The dominant role of the reaction thermal mode

Maksym Chylii, Liudmila Loghina, Anastasia Kaderavkova, Stanislav Slang, Jhonatan Rodriguez-Pereira, Bozena Frumarova and Miroslav Vlcek

Center of Materials and Nanotechnologies, Faculty of Chemical Technology, University of Pardubice, nam. Cs. Legii 565, Pardubice, 53002, Czech Republic

* The corresponding author's e-mail: Liudmila.Loghina@upce.cz

Abstract

Quite recently, nanosized rare-earth (RE) fluorides have been gaining importance due to their ability to form nanocomposites that are capable to absorb ionizing radiation. The efficiency of these materials may vary under the influence of external factors and under the growing conditions of nanocrystals. In this paper, a novel effective approach to the synthesis of CeF_3 nanocrystals (NCs) with a high yield of the desired material was proposed. The developed approach allows different modifications within the synthesis, thereby making it possible to change the growth conditions of QDs. The main exchange reaction between cerium oleate and ammonium fluoride was carried out in a non-coordinating solvent 1-octadecene (ODE) diluted with an excess of oleic acid (OA). The influence of the reaction temperature on the nucleation and the formation of a nanocrystals was presented. The possibility of introducing Tb^{3+} (1 - 5 %) into nanosized CeF_3 at one of the lowest reaction temperatures (180 °C) was also studied. The introduction of Tb^{3+} into the CeF_3 crystal lattice led to changes in the nanocrystal's structure, an increase in their size and also to the expected changes in the photoluminescence (PL) spectra. The prepared CeF_3 and CeF_3:Tb QDs were well dispersible in low-polar media, which makes them promising candidates for the role of active agents or wavelength shifters in the matrix of polymer scintillators.

Keywords: one-pot synthesis, CeF_3 NCs, CeF_3:Tb NCs, photoluminescence

1. Introduction

In recent decades, the scientific community has paid great attention to the study of ~~the~~ nanoscale materialsdue to their unique properties. Particular attention is given to the fluorescent materials based on rare earth elements (REE). Nanosized undoped and lanthanide-doped halides are widely used in medicine for drug delivery, bioimaging, X-ray therapy and MRI, [1–7] in the industry as components of solid-state lasers, lighting, displays, and LEDs [8–11], in high energy physics as converters of high-energy radiation to the visible region, as host materials of polymer-inorganic composites and as individual scintillators [12–15].

A significant feature of nanosized rare-earth fluorides is their ability to effectively absorb ultraviolet and higher energy radiation with the appearance of the emission in the visible part of the spectrum. Lanthanide-doping of RE-based NCs can significantly increase the intensity of photoluminescence. Thus, the probability of non-radiative relaxation of charge carriers decreases at low lattice phonon energy level (< 400 cm^{-1}), and, as a result, an increase in the intensity of photoluminescence is observed [7,16–18].

Currently, RE-based NCs are one of the most commonly used fluorescent host material in a polymer matrix. In this case, NCs must meet certain requirements, including uniformity in size and shape, chemical stability in the solid state and in the form of sols, and also good dispersibility in various types of solvents. In many ways, these properties are determined by the synthetic method. At present, such approaches as chemical precipitation from aqueous solutions, hydrothermal synthesis, molten salt synthesis, microemulsion synthesis, sonochemistry, *etc.* [7,15,19–23] are frequently used. Shcherbakov *et al.* [24] presented the synthesis of nano-sized fluorides CeF_3 and CeF_3:Tb, with an average diameter of ≈ 20 nm in the form of aqueous sols at room temperature. NCs synthesized by these methods are perfectly dispersed in aqueous media, which makes them favorable for various bio applications.

Among the presented in literature approaches to the preparation of RE-based nanomaterials, most of them lead to the production of large nanocrystals (with a diameter of 100 nm or more) or nanoparticles' agglomerates, which minimizes the ability to disperse. Nevertheless, CeF_3 nanoparticles of uniform size (≈ 15 nm) and shape (triangular nanoplates) were obtained by H. Sun *et al.* [25]. The authors suggested the use of RE trifluoroacetates, with their further decomposition at high temperatures (280 and 335 °C). The decomposition process of such salts is ambiguous even at high temperatures. S. Gai *et al.* also demonstrated a method for producing monodispersed (≈ 15 nm) CeF_3 and CeF_3:Tb nanoparticles based on oleates of the corresponding metals and NaF in 1-octadecene and oleic acid at high temperature (280 °C) [26]. C. Li *et al.* [27] presented the synthesis of water-dispersible CeF_3 and CeF_3:Tb nanoparticles (average diameter ≈ 10 nm) using the solvothermal method from cerium and terbium nitrates and NH_4F at 200 °C, using poly(ethyleneimine) as a stabilizer.

Most of the methods [25-27] described above are based on the exchange reaction, which reaches equilibrium under certain conditions. The equilibrium in the desired direction could be shifted in several ways, among which the most effective are increasing the temperature of synthesis and removal of one or more reaction products from the reaction medium. By using alkali metal fluorides in this reaction, the equilibrium also shifts toward the formation of a weak base salt. However, the removal of sodium or potassium salts from the system is difficult, especially if these salts are included in the crystal lattice of NCs. Usually, it leads to changes in the optical properties of the nanomaterials, decrease of the chemical resistance in air and destabilization of sols. For this reason, the development of an effective method for the preparation of stable, well-defined sizes and good dispersibility of RE-based fluorides is still on the table.

Here we propose a suitable strategy for the synthesis of CeF_3 NCs by eliminating the negative effects of alkali metal ions. - This approach involves the interaction of cerium oleate with ammonium fluoride in a non-coordinating solvent 1-octadecene, with an excess of oleic acid. Ammonia formed during the reaction has been removed from the system by Ar flow, which contributes to an equilibrium's shift towards the formation of CeF_3 NCs. Another advantage of this approach is its technological effectiveness. All stages of the synthesis, leading to the formation of NCs, are carried out in one flask, *i.e.* one-pot synthesis. We studied the growth temperature effect of NCs on their morphology and optical properties. It was shown that this reaction could lead to the formation of NCs at sufficiently low temperatures. Also, the possibility of CeF_3 NCs doping with another RE element at one of the lowest temperatures (180 °C) was investigated. The introduction of Tb^{3+} ions (1, 2, and 5 mol %) into the CeF_3 NCs crystal lattice led not only to the expected changes in the optical properties (red shift), but also had a significant effect on the sizes of NCs.

2. Experimental section

2.1 Materials

Cerium acetate monohydrate ($Ce(Ac)_3 \cdot H_2O$, 99 %), ammonium fluoride (NH_4F, 98 %), terbium acetate monohydrate ($Tb(Ac)_3 \cdot H_2O$, 99,9 %), oleic acid (OA, technical grade, 90 %) and 1-octadecene (ODE, technical grade, 90 %) were purchased from Sigma Aldrich Merck. Solvents were purchased from Lachner and used for the purification of NCs. Syntheses of NCs were carried out using standard Schlenk techniques under an Ar atmosphere.

2.2 Synthesis of CeF_3 NCs at different temperatures

Cerium acetate ($Ce(Ac)_3 \cdot H_2O$, 0.64 g, 0.002 mol), oleic acid (OA, 5 ml) and 1-octadecene (ODE, 5 ml) were placed into a Schlenk flask equipped with a thermometer. The mixture was degassed for 20 minutes at room temperature under constant stirring and then for another 30 minutes in the oil bath preheated to 100 °C. The purpose of the degassing process was in the elimination of air from the reaction system, as well as water vapor and acetic anhydride, which were formed by the anion replacement. At the end of degassing, the reaction flask was connected to Ar flow and the heating was discontinued. Further, ammonium fluoride (NH_4F, 0.22 g, 0.006 mol) was added into the spontaneously cooled reaction mixture (40 - 50 °C). After that, the reaction mixture was heated to the selected synthesis temperature (160 - 230 °C) under vigorous stirring, so that the heating rate was no higher than 5 °C/min. Aliquots were taken from the homogenized reaction

mixture (120 °C) and then every 10 °C while the temperature increased to follow the nucleation and growth of NCs. Upon reaching the selected synthesis temperature, aliquots were taken after 5, 10, 20 and 30 minutes. Aftewards, the heating was discontinued and the reaction mixture was allowed to cool spontaneously to 40 - 50 °C, after that the so-called "cold probe" was taken.

2.3 Synthesis of CeF_3:Tb NCs at 180 °C

Synthesis of Tb-doped CeF_3 NCs was carried out at 180 °C under the conditions described above. Calculated amounts of $Ce(Ac)_3 \cdot H_2O$ and $Tb(Ac)_3 \cdot H_2O$ with a total amount of 0.002 mol were added to the mixture of OA (5 ml) and ODE (5 ml). Tb doping was performed in the following molar ratios $Ce(Ac)_3 \cdot H_2O$: $Tb(Ac)_3 \cdot H_2O$ = 0.99 : 0.01; 0.98 : 0.02 and 0.95 : 0.05. After the addition of NH_4F (0.22 g, 0.006 mol), the reaction mixture was heated up to 180 °C with a constant rate of 5 °C/min. After that, heating at this temperature was kept for 30 minutes. Sampling was conducted according to a scheme similar to the previous synthesis.

2.4 Separation and purification of NCs

Separation and purification of CeF_3 and CeF_3:Tb NCs were performed under the same conditions. The cooled reaction mixture was transferred to an equivalent volume of cyclohexane and homogenized by mechanical stirring. Acetone (50 - 60 ml) was added in portions in the obtained colloidal solution. The precipitated NCs were separated by centrifugation (10 000 rpm / 7min), then they were *re*-dissolved in a minimal amount of cyclohexane and again precipitated with acetone. This *re*-dissolution-precipitation procedure was repeated three more times to separate CeF_3 NCs (or CeF_3:Tb NCs) from the ODE and unreacted precursors, following the further drying of NCs *in vacuo* for 4 hours. The dried NCs were additionally purified to separate the smallest crystals and stabilize the ligand shell. The dried nanocrystals were suspended in 10 ml of methanol and held for 15 minutes in an ultrasonic bath (room temperature, 37 kHz), following the separation and drying procedure described above. The product yield was in the range of 0.4 - 0.5 g.

2.5 Characterization

IR spectra in the region 4000 - 400 cm^{-1} (resolution 2 cm^{-1}) were recorded on Vertex 70v FT-IR spectrometer (Bruker, Germany) using single-bounce diamond ATR crystal. X-Ray diffraction patterns (XRD) were registered using PANalytical EMPYREAN powder X-ray diffractometer (ALMELO, Netherlands) with Cu-K_α radiation (λ = 1.5418 Å). Data were obtained across a 2θ range of 20 - 70° with a step size of 0.05°. The chemical composition of CeF_3 and Tb-doped CeF_3 NCs

was determined by X-Ray photoelectron spectroscopy (XPS, ESCA 2SR, Scienta-Omicron, Sweden) by monochromatic Al K_α source (1486.6 eV). Nanopowders were pressed into C tape for the XPS. The binding energy scale was referenced to adventitious carbon (284.8 eV) and the quantitative analysis was carried out using sensitivity factors provided by the manufacturer.

Energy dispersive X-Ray (EDX/EDS) spectroscopy was performed also to analyse the chemical composition of NCs using scanning electron microscope LYRA 3 (Tescan, Czech Republic) equipped with EDX detector AZtec X-Max 20 (Oxford Instruments, UK) at 20 kV acceleration voltage. The same device was used for STEM measurements using a retractable STEM detector (Tescan, Czech Republic) at 30 kV acceleration voltage.

The optical properties measurements of all synthesized CeF_3 and Tb-doped CeF_3 NCs were performed on Fluorometer PTI QuantaMaster 400 (Horiba, Germany) to obtain PL data in the spectral range 250 - 800 nm using excitation wavelength λ = 295 nm and UV-3600 (Shimadzu, Japan) spectrometer to get UV-VIS absorbance spectra in the spectral range 200 - 800 nm.

3. Results and discussion

3.1 Synthesis of CeF_3 and CeF_3:Tb NCs

The selection of synthesis conditions for CeF_3 NCs was determined by the requirements for the composition and optical properties of the final product. For our approach, we chose ammonium fluoride as a fluorinating agent. This inexpensive salt, which does not contain side active components capable of carrying out undesirable processes, is involved in the exchange reaction in a low-polar organic medium with the parallel formation of oleic acid amide and free ammonia (Figure 1).

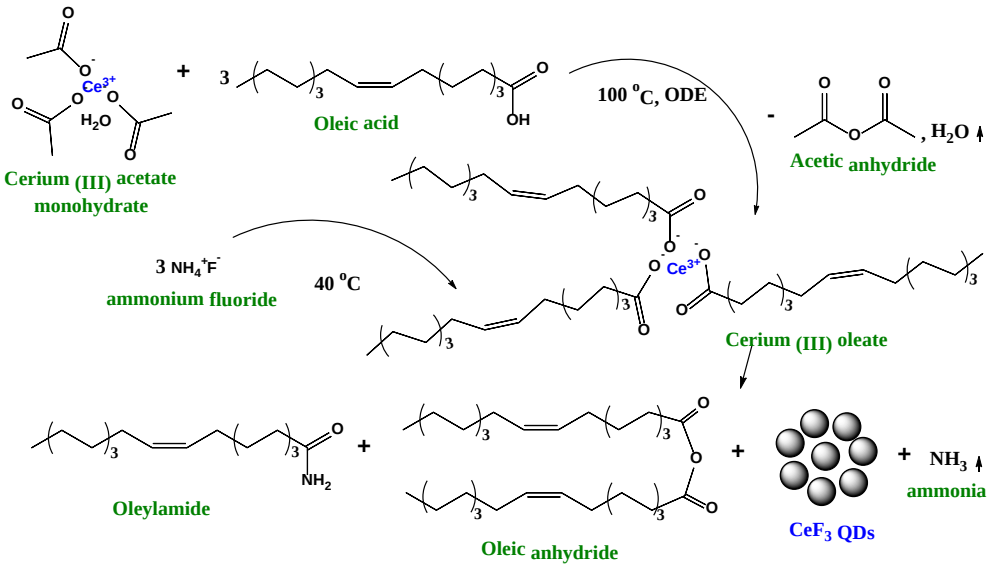

Figure 1. The general scheme of CeF_3 NCs synthesis.

The homogenization of all components, which is the most important factor for the successful and uniform NCs' growth, is hindered by their solubility in the reaction medium. Therefore, a soluble cerium salt is required for the exchange reaction in an organic medium (a mixture of ODE and OA). In this case, the most suitable candidates are carboxylates. Cerium oleate (as well as terbium oleate) was prepared *in situ* by the reaction between the corresponding acetate and oleic acid at 100 °C and continuous removal of the forming acetic anhydride and water vapor *in vacuo*. Organic *by*-products (oleylamide and oleic acid anhydride), which are formed during the reaction process, are not crystalline substances and can be easily removed during the cleaning process of NCs. Ammonia was removed under Ar flow.

The exchange reaction between cerium oleate and NH_4F, at some point, reaches the equilibrium, and saturation with molecular CeF_3 is created in the system. At this moment, the nucleation begins, which ensures the removal of nanocrystalline CeF_3 from the reaction volume and, accordingly, the equilibrium's shift. A constant concentration of molecular CeF_3 in the solution promotes further crystal growth. For better understanding and evaluation of the processes occurring in the reaction system, aliquots were taken from the reaction mixture. Before reaching the selected growth temperature, aliquots (30 µl volume) were taken every 10 °C and then at the 5th, 10th, 20th and 30th minute of the process. Further, aliquots were dissolved in 2 ml of cyclohexane. The measured absorbance spectra (ABS) and photoluminescence (PL) spectra of the CeF_3 NCs growth are presented in Figure 2.

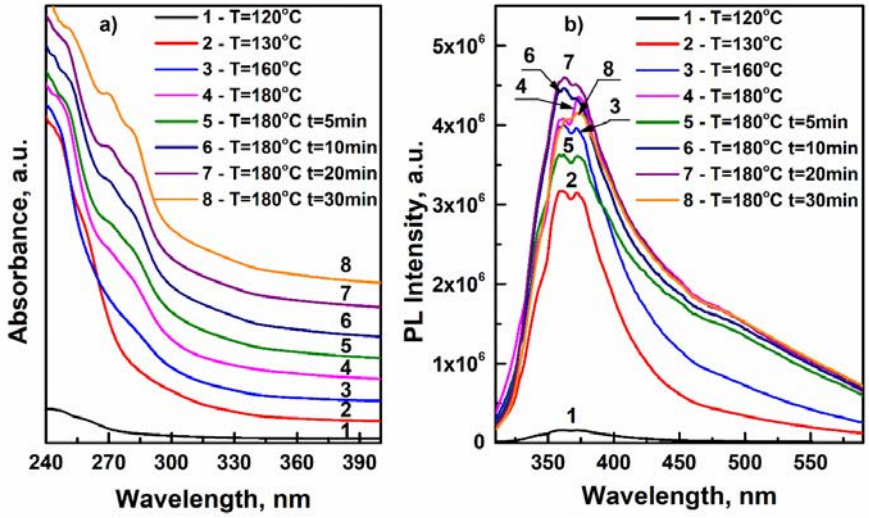

Figure 2. UV-VIS absorbance spectra (a) and photoluminescence (b) of the CeF_3 NCs growth.

It should be noted that there were no NCs' signals in the PL and ABS spectra until the reaction system reaches 130 °C. With a further increase in temperature, a change in the PL signal's intensity was observed. That confirms a stepwise shift in the equilibrium of the exchange reaction and the corresponding change in the NCs' concentration in the reaction mixture. In the ABS spectra, a small red shift of the first exciton can be seen, indicating a uniform growth of NCs. More details about the growth of CeF_3 and CeF_3:Tb NCs could be found in Supplementary materials, Fig. S2.

3.2 Structural analysis and morphology of synthesized CeF_3 and CeF_3:Tb NCs

3.2.1 XRD analysis and morphology of CeF_3 and CeF_3:Tb NCs

Figure 3a demonstrates the X-Ray diffractograms of prepared CeF_3 NCs at different temperatures. In the spectra were observed 8 peaks at 2θ values of 24.5, 24.9, 27.7, 35.1, 43.9, 45.1, 50.9, 52.9 corresponding to (002), (110), (111), (112), (030), (113), (032), (221) crystallographic planes. Indicated positions of *hkl* indices well match with the hexagonal structure of the bulk CeF_3 crystal phase (ICSD:42470) with a space group $P6_3/mcm$. The preferred orientation of the nanocrystals is along the (111) direction. It should be noted that due to the fine nanocrystalline nature of the NCs, the main peaks are broadened and it leads to the overlapping of the signals from the crystallographic planes. No peaks of secondary phases from impurities were found, confirming the high purity of the samples. Small inclusion of cubic phase was detected in all CeF_3 NCs, probably because of the low internal energy differences (< 20 meV per atom) between cubic and hexagonal phases. With a temperature growth, an increase in the Ce content per the unit cell appears, which leads to a tiny shift of the 3 main peaks at 2θ to the higher angles. According to the calculations of the average size by Scherrer's equation, a decrease in the nanocrystal sizes was detected [27]. The results of calculations of the lattice parameters and average crystal sizes are summarized in Table 1.

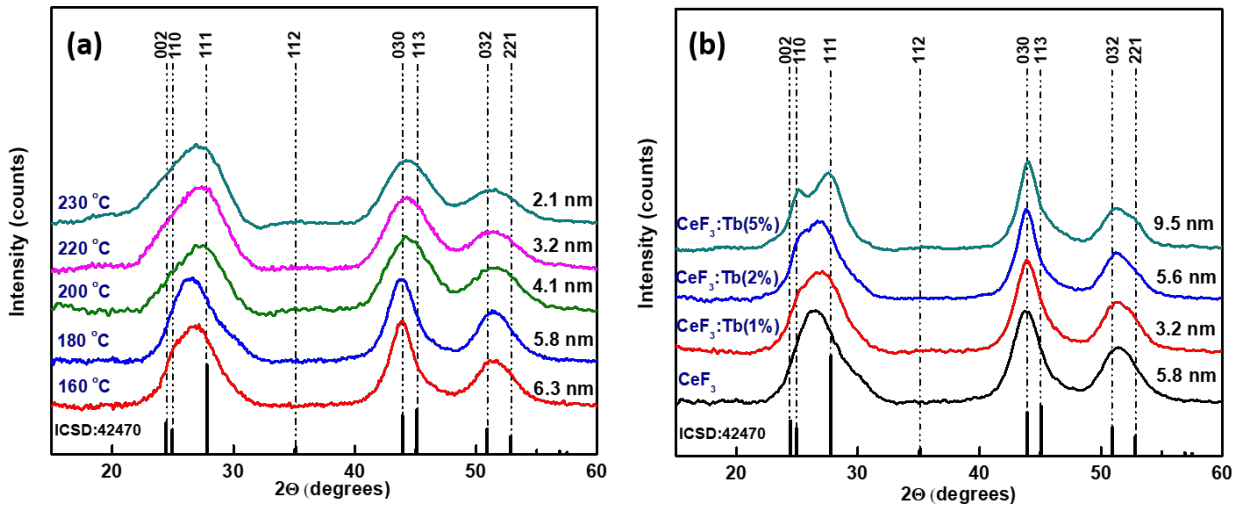

Figure 3. X-ray diffraction spectra of undoped CeF_3 NCs prepared at different temperatures (a) and Tb-doped CeF_3 NCs prepared at 180 °C (b).

The effect of Tb^{3+} doping on the crystal structure of CeF_3 NCs under the adopted conditions (180 °C) illustrated in Figure 3b. The X-Ray diffractograms of the Tb-doped CeF_3 NCs are similar to the undoped CeF_3 NCs, which confirms successful substitution of Ce^{3+} (1.01 Å) by Tb^{3+} (0.92 Å). All Tb-doped CeF_3 NCs can be indexed to the hexagonal crystal structure of CeF_3 with a space group $P6_3/mcm$, which is in good agreement with [26,28]. The continuous replacement of Ce^{3+} by Tb^{3+} brings a gradual shift of the diffraction peaks towards higher angles. The determined lattice parameters of Tb-doped CeF_3 NCs are getting smaller due to the smaller ionic radii of Tb^{3+}. Similar behavior of the crystal lattice was found by Liu *et al*. [23]. The average nanocrystalline sizes are listed in Table 2.

The shape of NCs and their sizes were also calculated from STEM images for 20 randomly selected NCs. Figures 4 and 5 demonstrate examples of these calculations. Tables 1 and 2 contain the results of the size calculations according to Scherrer's equation, and their comparison with average sizes calculated according to STEM.

Table 1. Structural parameters of CeF_3 NCs prepared at different temperatures

CeF_3 NCs	Mean crystalline size by XRD, nm	Size from STEM images		Space group	Lattice parameter	
		Length, nm	Width,nm		*a=b*, Å	*c*, Å
T=160 °C	3.1	12.5	4.7	$P6_3/mcm$	7.12571	7.18942
T=180 °C	3.1	12.2	3.8	$P6_3/mcm$	7.15522	7.23223
T=200 °C	2.4	8.9	2.6	$P6_3/mcm$	7.13877	7.29223
T=220 °C	2.2	3.5	3.5	$P6_3/mcm$	7.08847	7.27872
T=230 °C	2.1	2.8	2.8	$P6_3/mcm$	7.07590	7.27636

Table 2. Structural parameters of CeF_3:Tb NCs

NCs	Mean crystalline size by XRD, nm	Size from STEM images		Space group	Lattice parameter	
		Length, nm	Width,nm		*a=b*, Å	*c*, Å
CeF_3:Tb (1 %)	3.16	8.0	4.3	*P*6$_3$/*mcm*	7.14792	7.25113
CeF_3:Tb (2 %)	3.48	12.9	4.0	*P*6$_3$/*mcm*	7.14621	7.22086
CeF_3:Tb (5 %)	4.35	18.4	6.7	*P*6$_3$/*mcm*	7.12851	7.24521

As mentioned above, the nucleation of CeF_3 NCs occurred at rather low temperatures. By changing the synthesis temperature, we have influenced the level of NCs‘ saturation limit in the reaction medium. Therefore, with an increase of the colloidal solution temperature, the saturation level goes down, which leads to a decrease in the average size of CeF_3 NCs (Fig. 4). The CeF_3 NCs synthesized at 160 °C (Fig. 4a) have rice-shaped elongated grains, approximately 12.5 nm long and 4.7 nm wide. With a rise of the synthesis temperature to 200 °C (Fig. 4b-c), a decrease in the QD‘s size was observed with the preservation of the ellipse-like shape. However, the level of the ellipse‘s tension is gradually diminished. Further, with subsequent growth of the synthesis temperature to 220 °C and 230 °C, the shape of the CeF_3 NCs becomes almost spherical, and the size decreases to 3.5 nm and 2.8 nm, respectively.

Figure 5 represents the tendency to the growth of NCs, induced by an increase of terbium amount introduced into the crystal lattice. Comparing the STEM images of undoped CeF_3 NCs (Fig. 4b) and Tb-doped CeF_3 NCs prepared at 180 °C, it can be seen that the grain shape is preserved and their average length varies from 8.0 to 18.4 nm.

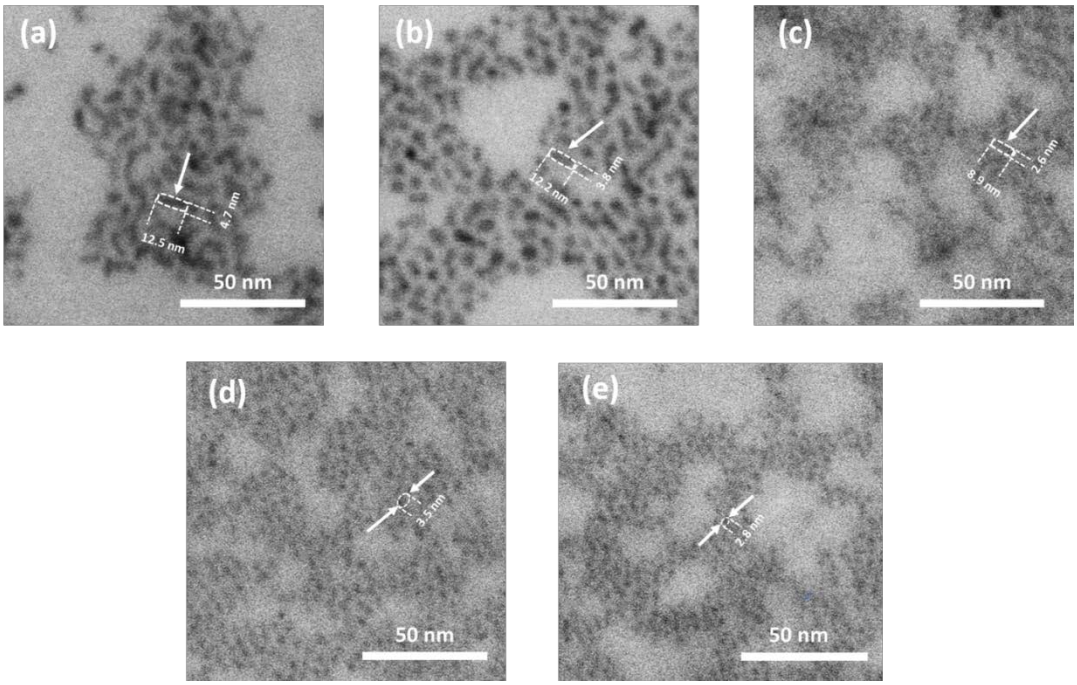

Figure 4. STEM images of undoped CeF_3 NCs synthesized at 160 °C (a), 180 °C (b), 200 °C (c), 220 °C (d), 230 °C (e).

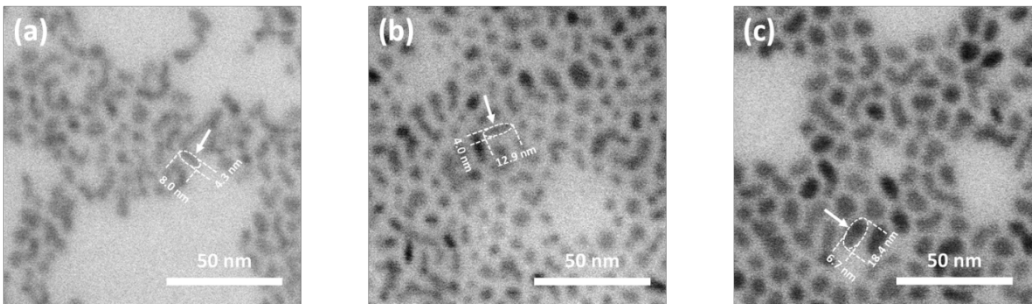

Figure 5. STEM images of Tb-doped CeF_3 NCs synthesized at 180 °C: a - CeF_3:Tb (1 %), b - CeF_3:Tb (2 %), c - CeF_3:Tb (5 %).

The elemental composition of CeF_3 NCs synthesized at different temperatures and Tb-doped CeF_3 NCs were measured by Energy dispersive X-ray (EDX/EDS) spectroscopy. The data are presented in Tables 3 and 4, respectively. As can be noticed from Table 3, Ce : F ratios in all the studied samples are close to stoichiometry. However, the protective shell of each quantum dot carries a certain number of cerium oleate molecules according to NCs size. Thus, with a rise of the QD's size and, accordingly, a change in the surface area per unit volume, the number of cerium carboxylate molecules also varies. Following the above, with a decrease of the NCs size, the Ce : F elemental ratio will increase toward the metal. The tendency in the cerium content growth with an augmentation in the synthesis temperature (Table 3) was observed, which in turn correlates with the indicated sizes of CeF_3 NCs.

Similar changes occurred in the ratio of the metals to fluorine in the elemental composition of Tb-doped CeF_3 NCs (Table 4). We suppose that the reactivity of the terbium precursor is higher than the cerium one, and the protective shell of the NCs consists of cerium oleate. Consequently, the terbium to cerium content in one quantum dot will be lower than that taken in synthesis. This hypothesis was supported by EDS analysis. EDS spectra for CeF_3 NCs prepared at 180 °C and Tb-doped CeF_3 NCs are presented in Supplementary materials (Fig. S3).

Table 3. Elemental composition of CeF_3 NCs prepared at different temperatures

CeF_3 NCs	Ce, at. %	F, at. %	Ce : F ratio
T=160 °C	22.40	77.60	1.00 :3.46
T=180 °C	25.31	74.69	1.00 :3.46
T=200 °C	29.68	70.32	1.00 :2.95
T=220 °C	29.59	70.41	1.00 :2.38
T=230 °C	31.49	68.51	1.00 :2.18

Table 4. Elemental composition of Tb-doped CeF_3 NCs

NCs	Ce, at. %	F, at. %	Tb, at. %	Ce : Tb ratio
CeF_3:Tb (1 %)	27.87	71.94	0.19	99.33 : 0.67
CeF_3:Tb (2 %)	23.76	75.83	0.41	98.30 : 1.70

CeF_3:Tb (5 %)	24.04	75.02	0.94	96.23 : 3.77

3.2.2 X-ray Photoelectron Spectroscopy

The surface chemical environment and composition of CeF_3 NCs in the presence and absence of Tb were investigated by XPS analysis. Through the survey spectra of undoped CeF_3 NCs obtained at different temperatures (Fig. 6a), we identified the presence of C, O, Ce and F. Furthermore, the intensity of the oxygen signal of the NCs increases from 200 °C onwards, while, the oxygen atomic concentration for NCs prepared at 200 °C, 220 °C and 230 °C is about three times higher than that of NCs at 160 °C and 180 °C (see Table S1). This phenomenon confirms the growing number of cerium carboxylates molecules surrounding the quantum dot with a rise of the synthesis temperature, and correspondingly, a decrease in the average QD size. Fig. 6b displays high resolution (HR) Ce *3d* spectra of undoped CeF_3 NCs prepared at various temperatures, where the corresponding spin-orbit Ce $3d_{5/2}$ / Ce $3d_{3/2}$ signals show a multiplet with two doublets. The first one was centered at 884.3 / 902.8 eV, and the second one was located at 887.5 / 905.9 eV. These binding energies (BEs) were attributed to the presence of Ce^{3+} containing into CeF_3 lattice [29]. F *1s* HR spectra for CeF_3 NCs are shown in Fig. 6c, where a single peak at 684.8 eV was observed. This BE corresponding to the existence of the Ce-F bond from semiconductor lattice [29]. Apparently, the temperature does not affect on the Ce and F binding energy of undoped NCs since all bands in the spectra are centered in the same energy.

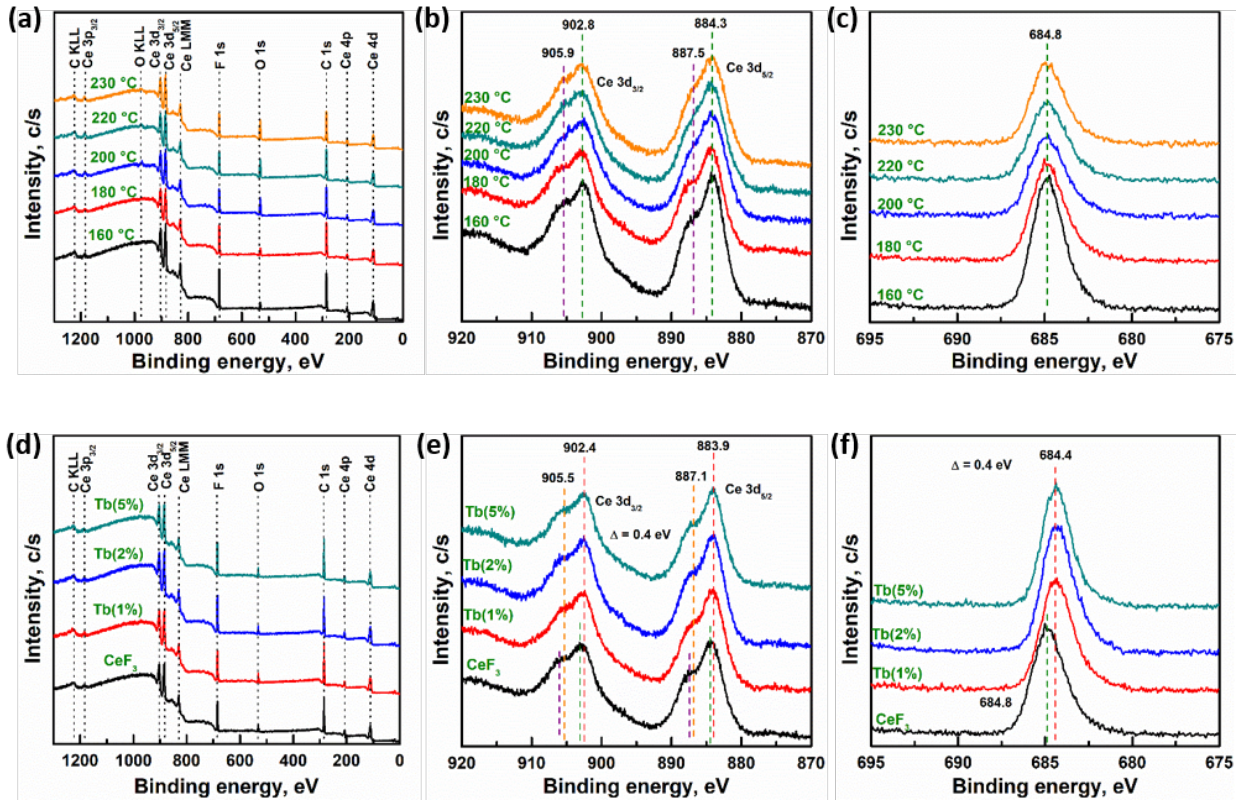

Figure 6. XPS spectra of undoped CeF_3 NCs, (a) survey, (b) Ce *3d* and (c) F *1s*; and Tb-doped CeF_3 with undoped CeF_3 at 180 °C NCs, (d) survey, (e) Ce *3d* and (f) F *1s*.

On the other hand, survey spectra of Tb-doped CeF_3 NCs with different doping percentages reveal the presence of C, O, Ce and F similar to undoped NCs (Fig. 6d). Their corresponding chemical composition is presented in Table S2 (Supplementary materials). In this case, we were not able to observe the main signal of Tb due to the surface sensitivity of the technique and the low concentration of this metal. HR Ce *3d* spectra of Tb-doped CeF_3 NCs are displayed in Fig. 6e. Interestingly, the spin-orbit Ce $3d_{5/2}$ / Ce $3d_{3/2}$ signals of this material presented a lower BE compared with those of the unmodified CeF_3 (around 0.4 eV), suggesting that the existence of Tb produces modification in the chemical environment. We suggest the incorporation of Tb^{3+} in substitutional positions of Ce^{3+} into CeF_3 lattice [18]. Doublets were centered at 883.9 / 902.4 eV, and 887.1 / 905.5 eV, respectively. Similarly, the HR F *1s* spectra of doped NCs (Fig. 6f) also show a shift around 0.4 eV on the signal centered at 684.3 eV. Even though Tb^{3+} was not directly detected by XPS, the modification of the Ce-F bonds allows deducing that a low fraction of Tb^{3+} was introduced into CeF_3 matrix.

3.2.3 FT-IR spectral studies of CeF_3 and CeF_3:Tb NCs

The presence of the OA-containing ligands, which are important in the preparation of NCs with long-time stability, can be confirmed by measuring infrared spectra. The ATR spectra of CeF_3 and

CeF_3:Tb NCs are presented in Fig. 7. Characteristic vibrations in the region between 3600 and 500 cm^{-1} correspond to organic species (OA) and between 500 and 50 cm^{-1} - to inorganic salts. All the spectra were scaled by the maximum intensity of the absorbance band corresponding to the vibrations modes of NCs.

In all spectra of our samples, visible absorbance bands were detected, which can be assigned to characteristic modes of oleyl groups [30–32]. Bands in the region of 3050 - 2800 cm^{-1} were attributed to the symmetric and asymmetric stretching vibrations of $-CH_2-$ and CH_3- groups: 3005 cm^{-1} (ν CH in -CH=CH- group), 2954 cm^{-1} (ν_{as} $-CH_3$), 2922 cm^{-1} (ν_{as} $-CH_2-$), 2851 cm^{-1} (ν_s $-CH_2-$). In the fingerprint region, the absorbance band at 722 cm^{-1} confirms the presence of $(CH_2)_n$ alkyl chains with n > 4. The peak associated with C=C mode is very weak and in our case is visible either as a shoulder at 1650 cm^{-1} or is hidden in an absorbance band with maxima at 1707 cm^{-1}. This band at 1707 cm^{-1} can be assigned either to the carbonyl stretching mode (C=O) of oleic acid or to asymetric vibrations of unidentate carboxylates [26,33–35].

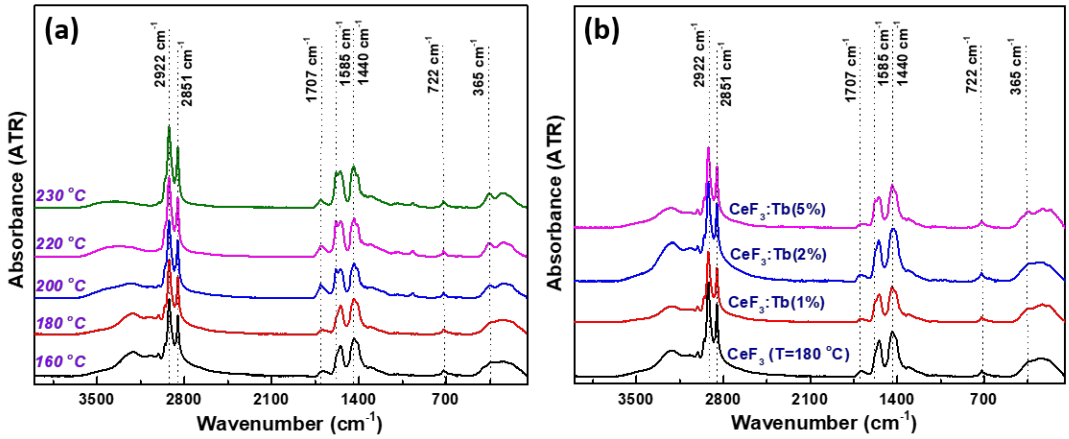

Figure 7. FT-IR spectra of prepared at different temperatures CeF_3 NCs (a) and Tb doped CeF_3:Tb (1-5 %) NCs (b).

In the region of characteristic COO^- frequencies, the strong peaks corresponding to asymmetric (1585 and 1548 cm^{-1}) and symmetric (1438 and 1412 cm^{-1} (shoulder)) stretches of carboxylate groups were observed. Shoulders at 1466 and 1455 cm^{-1} belong to deformation $-CH_3$ and $-CH_2-$ vibrations. The carboxylate ion may coordinate to metal in four different modes: ionic, unidentate (Δ = 200 - 300 cm^{-1}), bidentate (Δ < 110 cm^{-1}) and bridging (Δ = 110 - 200 cm^{-1}) [36,37]; the Δ is difference between positions of asymmetric and symmetric stretching vibrations of COO^- group ($\Delta = \nu_{as} - \nu_s$). In the case of samples prepared at lower reaction temperatures (160 and 180 °C), the band with maxima at 1547 cm^{-1} is dominant in the region of asymmetric carboxylate COO^- vibrations. The vibration band at 1585 cm^{-1} forms only a faintly visible shoulder. The differences between band at 1547 cm^{-1} and two bands at 1440 and 1412 cm^{-1} indicate the

presence of namely bridging coordination (Δ = 110 and 136 cm^{-1}). In the case of samples prepared at higher synthesis temperatures (200, 220 and 230 °C), the intensity of the band at 1585 cm^{-1} is greatly increasing due to the presence of another coordination mode. The Δ values are 145 and 173 cm^{-1} also suggest bridging coordination and probably also unidentate coordination of oleate ligands. However, the Δ = 173 cm^{-1} is lower than the values given for unidentate coordination. It could be caused by the hydrogen bonding of non-coordinated carboxylate oxygen with the hydroxyl group of the free oleic acid, which leads to a "pseudo bridged" unidentate arrangement [37]. The approximately similar intensity of bands at 1585 and 1548 cm^{-1} could indicate the presence of both bridging and unidentate coordination of oleate ligands when high reaction temperatures are applied during the synthesis of CeF_3 NCs. The shoulder at 1740 cm^{-1}, which appears in the spectra of samples synthesized at higher temperatures, probably belongs to C=O stretching vibrations of the unidentate ligand [37].

A relatively strong and wide band between 500 and 50 cm^{-1} corresponds to the fundamental vibration of CeF_3 NCs. A similar band was observed in transmission and reflection spectra of cerium (III) fluoride and other RE fluorides [38–41]. It is evident that the wide absorbance band in our spectra is composed of at least 5 bands, which are probably associated with A_{2u} and E_{1u} infrared active modes in CeF_3 with D_{6h}^3 ($P6_3/mcm$) symmetry.

3.3 Optical properties of CeF_3 and CeF_3:Tb NCs

3.3.1 Optical properties of CeF_3 NCs prepared at different temperatures

For the measurement of optical properties, the studied NCs were dispersed in cyclohexane so that the optical density of the obtained sols was no more than 1. Figure 8 demonstrates the ABS (a) and PL (b) spectra of CeF_3 NCs synthesized in the temperature range of 160 - 230 °C. A wide band with a maximum at 280 nm was observed in the ABS spectra of CeF_3 NCs synthesized at 160 °C (Fig. 8a). By increasing the synthesis temperature, a slight red shift of this signal with an increase in its intensity was detected. In our opinion, this signal corresponds to the position of the first exciton in CeF_3 NCs. The PL emission spectra of CeF_3 NCs synthesized in 160 - 230 °C temperature range were measured under λ_{exc} = 295 nm at room temperature. As follows from Figure 8b, the photoluminescence of the synthesized CeF_3 NCs represents a wide PL band in the range of 320 - 600 nm. It should be noted that a stable shift of the PL maximum's position occurs with an increase in the synthesis temperature. So, for CeF_3 NCs synthesized at 160 °C, the PL emission spectrum consists of two bands with PL maxima at 361 nm and 500 nm. The PL band at 361 nm for NCs synthesized at 160 °C belongs to the 5d - 4f luminescent transitions of the

"perturbed" Ce^{3+} [26,42,43]. At the same time, for CeF_3 NCs synthesized at 230 °C, the PL emission spectrum is represented by a single band with a maximum at 381 nm. The position of the PL band with a maximum at ≈ 500 nm is very close to the PL band of CeO_2 [44]. However, the presence of oxide in the QD's body was excluded based on the XPS analysis (Fig. 6), because the corresponding signal at 531.51 - 531.76 eV in the XPS spectrum refers to oxygen bound to carbon. Therefore, the presence of this PL emission band can be caused only by a growing number of surface defects. By raising the temperature, a decrease in the size of CeF_3 NCs, and as a consequence, an increase in the influence of the surface defects on the photoluminescence were observed. It leads to the expansion of the PL bands and the shift of the PL maximum to the long-wavelength region for CeF_3 NCs synthesized at 220 - 230 °C.

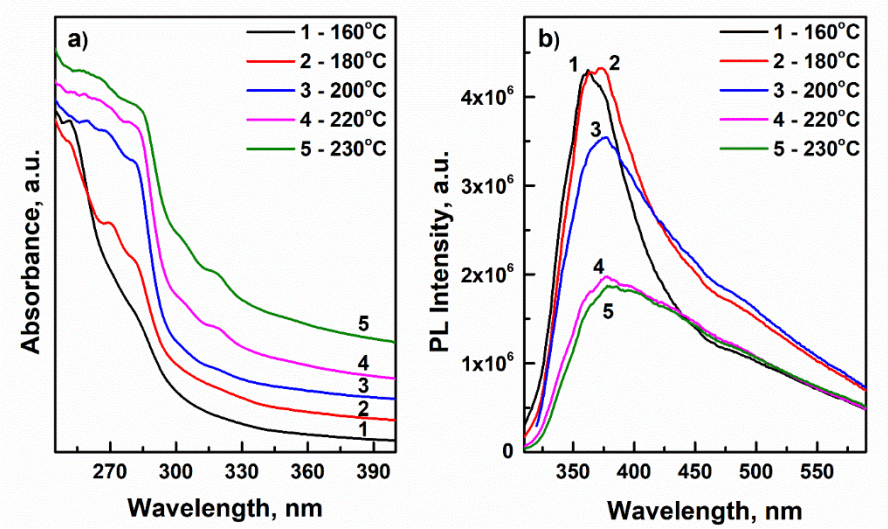

Figure 8. Absorbance (a) and PL emission (b) spectra of CeF_3 NCs synthesized at different temperatures.

One of the advantages of CeF_3 NCs is the large value of the Stokes shift (≈ 10 000 cm^{-1}). With an increase in the Stokes shift, the probability of concentration quenching during energy migration processes decreases [18]. For a better illustration and calculation of the Stokes shifts, the combined spectra of PL and ABS CeF_3 NCs prepared at different temperatures are presented in Fig. 9. There is a visible increase in the Stokes shift from 85 to 96 nm with a growth of the synthesis temperature. Such a change was caused by the shift of the PL maximum to the red region of the spectrum for CeF_3 NCs obtained at higher temperatures. The PL maxima's position, first transitions in the absorbance spectra and the calculated values of Stokes shift are presented in Table 5.

Using the ABS spectrum and the Tauc's equation derived for NCs [45], the band gap was estimated for CeF_3 NCs synthesized at different temperatures (Table 5). Graphical illustration of the band gap estimation is presented in Supplementary materials (Fig. S4).

Figure 9. Stokes shift plots of CeF_3 NCs prepared at different temperatures.

Table 5. Optical properties of CeF_3 NCs prepared at different temperatures. PL emission maximum (λ_{PL}), peak maximum of the first transition in the ABS spectra (λ_{ABS}), Stokes shift and band gap (E_g)

CeF_3 NCs	λ_{PL}, nm	λ_{ABS}, nm	Stokes shift, nm	E_g, eV
T=160 °C	361	281	80	4.16
T=180 °C	373	283	90	4.21
T=200 °C	377	282	95	4.24
T=220 °C	378	283	95	4.23
T=230 °C	381	285	96	4.16

3.3.2 Optical properties of Tb-doped CeF_3 NCs

As mentioned earlier, cerium fluoride is a good matrix for doping with other REs. The reason for this is the low energy of optical phonons, which reduces the probability of nonradiative relaxation of charge carriers [7]. Also, a contribution of the large Stokes shift is significant, which leads to a reduced probability of concentration quenching during energy migration [18]. Figure 10 represents the scheme of electronic transitions and a possible path for the excitation energy transfer from Ce^{3+} to Tb^{3+}.

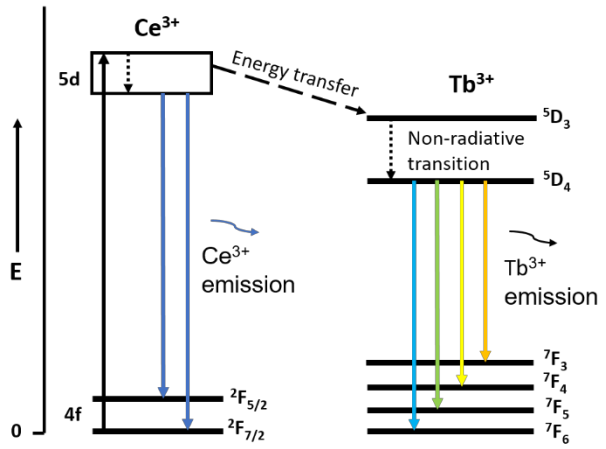

Figure 10. The proposed energy level diagram of CeF_3:Tb with the electronic transition and energy transfer process from Ce^{3+} to Tb^{3+}.

It is known that the efficiency of direct excitation of photoluminescent $4f^n$ transitions in RE salts is low due to their partial prohibition by transition rules. Therefore, another reason for using cerium fluoride as a matrix for introducing other REs, including Tb, is the high efficiency of energy transfer from Ce to REs elements, which leads to a significant increase in PL intensity [18].

Figure 11 illustrates the spectra of ABS (a) and PL (b) Tb-doped CeF_3 NCs synthesized at 180 °C. According to the ABS spectra, the introduction of terbium does not significantly affect the position of the first transition. At the same time, the PL spectrum changes are visible even with the 1 % of Tb doping (Fig. 11b).

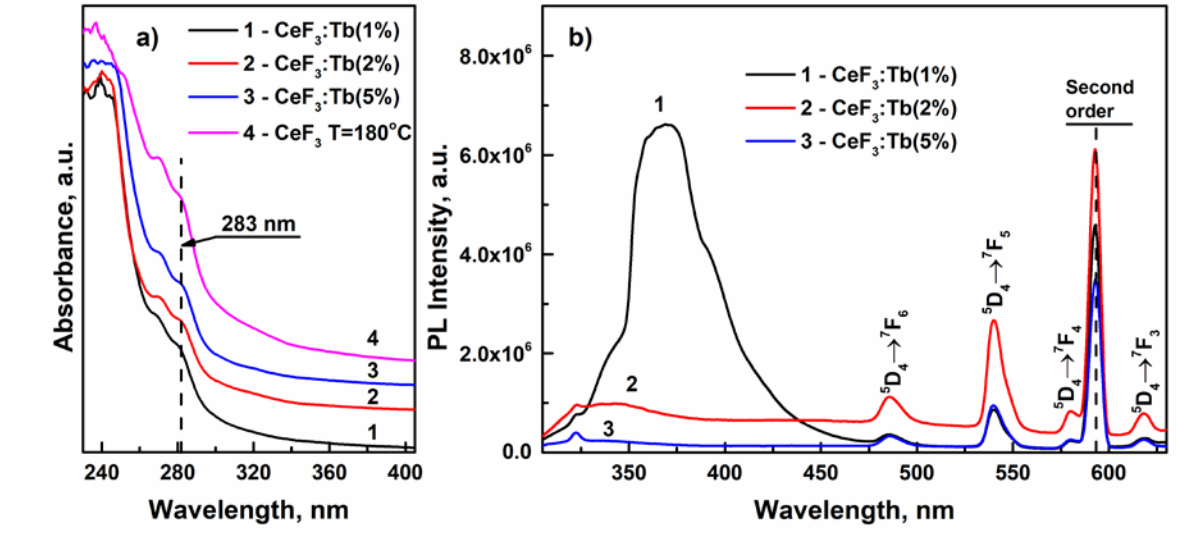

Figure 11. Absorbance (a) and photoluminescence emission (b) spectra of Tb-doped CeF_3 NCs.

The PL spectra presented in Fig. 11b were measured under λ_{exc} = 295 nm at room temperature. As can be seen from Figure 11b, several bands were detected with 1 % of Tb doping: PL bands from the Ce^{3+} ion at λ_{max} = 370 nm and PL bands belonging to $^5D_4$-$^7F_6$ (486 nm), $^5D_4$-$^7F_5$ (540 nm), $^5D_4$-$^7F_4$ (580 nm), and $^5D_4$-$^7F_3$ (618 nm) characteristic f-f transitions of Tb^{3+} ion. With a further rise

of Tb content in CeF_3 NCs, the intensity of the Ce^{3+} PL band decreases with a shift of PL maximum to 320 nm. At the same time, the PL transition intensity from Tb^{3+} increases, while maintaining the positions of the maxima. Thus, with an augmentation of Tb content in CeF_3 NCs, the efficiency of excitation energy transfer from Ce^{3+} to Tb^{3+} increases.

Conclusion

This paper has demonstrated the novel tuneable approach to the synthesis of highly photoluminescent and uniform CeF_3 NCs based on the interaction of *in situ* obtained cerium oleate with ammonium fluoride in a non-coordinating solvent of 1-octadecene. The effect of the synthesis temperature on the morphology, structure, and optical properties of NCs was investigated. The results of this study indicate that although nucleation occurs at sufficiently low temperatures (120 - 130 °C), the growth dynamics of NCs directly depends on the temperature of the reaction medium. It should be noted that with a rise of the synthesis temperature from 160 °C to 230 °C, the average QD size drastically decreases from 12.5 nm to 2.8 nm. The findings suggest that our approach could also be applied to the introduction of additional RE elements into the CeF_3 NCs matrix. This possibility has been studied using low concentrations of terbium. Doping was carried out at one of the lowest temperatures (180 °C), which made it possible to evaluate the effect of the concentration of Tb^{3+} ions on the size of NCs and their optical properties. The success of the doping was confirmed by EDS analysis data and also the appearance of characteristic bands of the Tb^{3+} ion in the PL spectra of CeF_3 NCs. Good dispersibility in non-polar media, intense photoluminescence, uniformity and small size of undoped and Tb-doped CeF_3 NCs give them a great potential for the introduction into inorganic-plastic mixed scintillators as a fluorescent host material for radiation detectors, light sensors, LEDs and other optical devices production.

Declaration of competing interest

The authors declare that they have no known competing financial interests or personal relationships that could have appeared to influence the work reported in this paper.

Acknowledgements

Authors appreciate financial support from project “High-sensitive and low-density materials based on polymeric nanocomposites” - NANOMAT (№ CZ.02.1.01/0.0/0.0/17_048/0007376), support from the grants LM2018103 and ED4.100/11.0251 from the Ministry of Education, Youth and Sports of the Czech Republic.

References

[1] M. Liu, H. Liu, S. Sun, X. Li, Y. Zhou, Z. Hou, J. Lin, Multifunctional hydroxyapatite/Na(Y/Gd)F_4:Yb^{3+}, Er^{3+} composite fibers for drug delivery and dual modal imaging, Langmuir. 30 (2014) 1176–1182. doi:10.1021/la500131d.

[2] F. Vetrone, J.A. Capobianco, Lanthanide-doped fluoride nanoparticles: Luminescence, upconversion, and biological applications, Int. J. Nanotechnol. 5 (2008) 1306–1339. doi:10.1504/IJNT.2008.019840.

[3] Y. Liu, W. Chen, S. Wang, A.G. Joly, Investigation of water-soluble x-ray luminescence nanoparticles for photodynamic activation, Appl. Phys. Lett. 92 (2008) 1–4. doi:10.1063/1.2835701.

[4] F. Evanics, P.R. Diamente, F.C.J.M. Van Veggel, G.J. Stanisz, R.S. Prosser, Water-soluble GdF_3 and GdF_3/LaF_3 nanoparticles - Physical characterization and NMR relaxation properties, Chem. Mater. 18 (2006) 2499–2505. doi:10.1021/cm052299w.

[5] N.J.J. Johnson, W. Oakden, G.J. Stanisz, R. Scott Prosser, F.C.J.M. Van Veggel, Size-tunable, ultrasmall $NaGdF_4$ nanoparticles: Insights into their T_1 MRI contrast enhancement, Chem. Mater. 23 (2011) 3714–3722. doi:10.1021/cm201297x.

[6] E.N.M. Cheung, R.D.A. Alvares, W. Oakden, R. Chaudhary, M.L. Hill, J. Pichaandi, G.C.H. Mo, C. Yip, P.M. MacDonald, G.J. Stanisz, F.C.J.M. Van Veggel, R.S. Prosser, Polymer-stabilized lanthanide fluoride nanoparticle aggregates as contrast agents for magnetic resonance imaging and computed tomography, Chem. Mater. 22 (2010) 4728–4739. doi:10.1021/cm101036a.

[7] D. González-Mancebo, A.I. Becerro, T.C. Rojas, A. Olivencia, A. Corral, M. Balcerzyk, E. Cantelar, F. Cussó, M. Ocaña, Room temperature synthesis of water-dispersible Ln^{3+}:CeF_3 (Ln = Nd, Tb) nanoparticles with different morphology as bimodal probes for fluorescence and CT imaging, J. Colloid Interface Sci. 520 (2018) 134–144. doi:10.1016/j.jcis.2018.03.007.

[8] M. Shang, G. Li, X. Kang, D. Yang, D. Geng, J. Lin, Tunable luminescence and energy transfer properties of Sr_3AlO_4F:RE^{3+} (RE = Tm/Tb, Eu, Ce) phosphors, ACS Appl. Mater. Interfaces. 3 (2011) 2738–2746. doi:10.1021/am200534u.

[9] G. Li, D. Geng, M. Shang, C. Peng, Z. Cheng, J. Lin, Tunable luminescence of Ce^{3+}/Mn^{2+} - coactivated $Ca_2Gd_8(SiO_4)_6O_2$ through energy transfer and modulation of excitation: Potential single-phase white/yellow-emitting phosphors, J. Mater. Chem. 21 (2011) 13334–13344. doi:10.1039/c1jm11650a.

[10] H. Guan, G. Liu, J. Wang, X. Dong, W. Yu, Multicolor tunable luminescence and paramagnetic properties of $NaGdF_4$:Tb^{3+}/Sm^{3+} multifunctional nanomaterials, Dalt. Trans. 43 (2014) 10801–10808. doi:10.1039/c4dt00158c.

[11] D. Li, Q. Ma, Y. Song, X. Xi, X. Dong, W. Yu, J. Wang, G. Liu, Tunable multicolor luminescence and white light emission realized in Eu^{3+} mono-activated GdF_3 nanofibers with paramagnetic performance, RSC Adv. 6 (2016) 113045–113052. doi:10.1039/c6ra21039b.

[12] T.J. Hajagos, C. Liu, N.J. Cherepy, Q. Pei, High-Z Sensitized Plastic Scintillators: A Review, Adv. Mater. 30 (2018). doi:10.1002/adma.201706956.

[13] C. Dujardin, D. Amans, A. Belsky, F. Chaput, G. Ledoux, A. Pillonnet, Luminescence and scintillation properties at the nanoscale, IEEE Trans. Nucl. Sci. 57 (2010) 1348–1354. doi:10.1109/TNS.2009.2035697.

[14] Y. Chen, C. Liu, Y. Jin, T.J. Hajagos, D. Kishpaugh, Q. Zhuang, Q. Pei, Ytterbium fluoride loaded plastic scintillators for γ-ray spectroscopy, Hard X-Ray, Gamma-Ray, Neutron Detect. Phys. XVIII. 9968 (2016) 99680N. doi:10.1117/12.2238336.

[15] M. Karimi, M. Raeisi, M. Bagherzadeh, F. Payami, Enhancement in photoluminescence properties of organic compound PS/PPO by cerium fluoride nanoparticles doping, SN Appl. Sci. 1 (2019) 1–6. doi:10.1007/s42452-019-0658-2.

[16] Y. Song, Y. Li, T. Zhao, Y. Wang, T. Cui, Y. Sheng, K. Zheng, X. Zhou, H. You, H. Zou, Facile synthesis and color-tunable properties of $BaLuF_5$:Ce,Tb,Eu(Sm) submicrospheres via a facile ionic liquid/EG two-phase system, J. Colloid Interface Sci. 487 (2017) 281–288. doi:10.1016/j.jcis.2016.10.044.

[17] H. Ahmadi, M. Bagherzadeh, M. Raeisi, F. Payami, Preparation and characterization and photoluminescence properties of CeF_3@ZnS nanocomposites, J. Mater. Sci. Mater. Electron. 31 (2020) 3215–3220. doi:10.1007/s10854-020-02869-y.

[18] X. Li, W. Zhang, L. Dong, D. Liu, Z. Qi, Low temperature molten salt synthesis of CeF_3 and CeF_3:Tb^{3+} phosphors with efficient luminescence properties, J. Lumin. 205 (2019) 122–128. doi:10.1016/j.jlumin.2018.08.067.

[19] Y. Liu, Y. Zhao, H. Luo, Z. Wu, Z. Zhang, Hydrothermal synthesis of CeF_3 nanocrystals and characterization, J. Nanoparticle Res. 13 (2011) 2041–2047. doi:10.1007/s11051-010-9958-6.

[20] M. Runowski, S. Lis, Synthesis of lanthanide doped CeF_3:Gd^{3+}, Sm^{3+} nanoparticles, exhibiting altered luminescence after hydrothermal post-treatment, J. Alloys Compd. 661 (2016) 182–189. doi:10.1016/j.jallcom.2015.11.182.

[21] J. Ladol, H. Khajuria, R. Singh, V. Kumar, H.N. Sheikh, Organic additive assisted hydrothermal synthesis and photoluminescence properties of CeF_3:Tb^{3+} and $NaCeF_4$:Tb^{3+} nanoparticles, J. Mater. Sci. Mater. Electron. 28 (2017) 11671–11681. doi:10.1007/s10854-017-6970-y.

[22] L. Wang, W. Zhang, Y. Zhao, L. Cao, Fabrication of silver nanoparticles loaded flowerlike CeF_3 architectures and their antibacterial activity, J. Phys. Chem. Solids. 120 (2018) 154–160. doi:10.1016/j.jpcs.2018.04.042.

[23] S. Liu, Y. Hui, L. Zhu, X. Fan, B. Zou, X. Cao, Synthesis and luminescence properties of CeF_3:Tb^{3+} nanodisks via ultrasound assisted ionic liquid method, J. Rare Earths. 32 (2014) 508–513. doi:10.1016/S1002-0721(14)60100-9.

[24] A.B. Shcherbakov, N.M. Zholobak, A.E. Baranchikov, A. V. Ryabova, V.K. Ivanov, Cerium fluoride nanoparticles protect cells against oxidative stress, Mater. Sci. Eng. C. 50 (2015) 151–159. doi:10.1016/j.msec.2015.01.094.

[25] X. Sun, Y.W. Zhang, Y.P. Du, Z.G. Yan, R. Si, L.P. You, C.H. Yan, From trifluoroacetate complex precursors to monodisperse rare-earth fluoride and oxyfluoride nanocrystals with diverse shapes through controlled fluorination in solution phase, Chem. - A Eur. J. 13 (2007) 2320–2332. doi:10.1002/chem.200601072.

[26] S. Gai, P. Yang, X. Li, C. Li, D. Wang, Y. Dai, J. Lin, Monodisperse CeF_3, CeF_3: Tb^{3+}, and CeF_3: Tb^{3+}@LaF_3 core/shell nanocrystals: Synthesis and luminescent properties, J. Mater. Chem. 21 (2011) 14610–14615. doi:10.1039/c1jm12419f.

[27] C. Li, F. Li, T. Li, T. Bai, L. Wang, Z. Shi, S. Feng, A facile synthesis and photoluminescence properties of water-dispersible Re^{3+} doped CeF_3 nanocrystals and solid nanocomposites with polymers, Dalt. Trans. 41 (2012) 4890–4895. doi:10.1039/c2dt30064h.

[28] F.N. Sayed, V. Grover, K.A. Dubey, V. Sudarsan, A.K. Tyagi, Solid state white light emitting systems based on CeF_3: RE^{3+} nanoparticles and their composites with polymers, J. Colloid Interface Sci. 353 (2011) 445–453. doi:10.1016/j.jcis.2010.10.005.

[29] D. Barreca, A. Gasparotto, C. Maccato, C. Maragno, E. Tondello, Cerium (III) Fluoride Thin Films by XPS, Surf. Sci. Spectra. 13 (2006) 87–93. doi:10.1116/11.20070202.

[30] G. Socrates, Infrared and Raman characteristic group frequencies. Tables and charts, 2001. doi:10.1002/jrs.1238.

[31] N.B. Colthup, L.H. Daly, S.E. Wiberley, CHAPTER 9 - CARBONYL COMPOUNDS, in: N.B. Colthup, L.H. Daly, S.E. Wiberley (Eds.), Introd. to Infrared Raman Spectrosc. (Third Ed., Third Edit, Academic Press, San Diego, 1990: pp. 289–325. doi:https://doi.org/10.1016/B978-0-08-091740-5.50012-0.

[32] L. Robinet, M.C. Corbeil, The characterization of metal soaps, Stud. Conserv. 48 (2003) 23–40. doi:10.1179/sic.2003.48.1.23.

[33] N. Agrawal, H. Bhatia, S. Anand, M.N. Gandhi, Detailed Photoluminescence Study of Dopedand Co-Doped CeF_3:RE^{3+} (RE^{3+} : Nd^{3+}, Sm^{3+}, Eu^{3+}, Gd^{3+}, Tb^{3+}, Dy^{3+}, Ho^{3+}, Er^{3+},Tm^{3+}, Int. J. Innov. Res. Sci. Eng. Technol. 2015 (2015) 9389–9402.

[34] L.M. Bronstein, X. Huang, J. Retrum, A. Schmucker, M. Pink, B.D. Stein, B. Dragnea, Influence of iron oleate complex structure on iron oxide nanoparticle formation, Chem. Mater. 19 (2007) 3624–3632. doi:10.1021/cm062948j.

[35] L. Wang, M. Zhang, X. Wang, W. Liu, The preparation of CeF_3 nanocluster capped with oleic acid by extraction method and application to lithium grease, Mater. Res. Bull. 43 (2008) 2220–2227. doi:10.1016/j.materresbull.2007.08.024.

[36] K. Nakamoto, Infrared and Raman Spectra of Inorganic and Coordination Compounds, John Wiley & Sons, Inc., Hoboken, NJ, USA, 2008. doi:10.1002/9780470405840.

[37] T. Balakrishnan, M.J. Lee, J. Dey, S.M. Choi, Sub-nanometer scale size-control of iron oxide nanoparticles with drying time of iron oleate, CrystEngComm. 21 (2019) 4063–4071. doi:10.1039/c9ce00112c.

[38] R.A. Nyquist, R.O. Kagel, INFRARED SPECTRA OF INORGANIC COMPOUNDS: in R.A. Nyquist, R.O. Kagel (Eds.), Handbook of Infrared and Raman Spectra of Inorganic Compounds and Organic Salts, Academic Press, New York, 1971: pp. 1–18. doi:10.1016/b978-0-12-523450-4.50005-5.

[39] G.N. Kustova, L.R. Batsanova, Infrared spectra of rare-earth metal fluorides in the region of a cesium iodide prism, J. Appl. Spectrosc. 4 (1966) 62–63. doi:10.1007/BF01106206.

[40] R.P. Bauman, S.P.S. Porto, Lattice vibrations and structure of rare-earth fluorides, Phys. Rev. 161 (1967) 842–847. doi:10.1103/PhysRev.161.842.

[41] H.H. Caspers, R.A. Buchanan, H.R. Marlin, Lattice vibrations of LaF_3, J. Chem. Phys. 41 (1964) 94–99. doi:10.1063/1.1725657.

[42] C. Li, X. Liu, P. Yang, C. Zhang, H. Lian, J. Lin, LaF_3, CeF_3, CeF_3:Tb^{3+}, and CeF_3:Tb^{3+}@LaF_3 (Core−Shell) Nanoplates: Hydrothermal Synthesis and Luminescence Properties, J. Phys.

Chem. C. 112 (2008) 2904–2910. doi:10.1021/jp709941p.

[43] F. Chaput, F. Lerouge, A.L. Bulin, D. Amans, M. Odziomek, A.C. Faure, M. Monteil, I. Dozov, S. Parola, F. Bouquet, M. Lecouvey, P. Davidson, C. Dujardin, Liquid-Crystalline Suspensions of Photosensitive Paramagnetic CeF_3 Nanodiscs, Langmuir. 35 (2019) 16256–16265. doi:10.1021/acs.langmuir.9b02335.

[44] Y. Malyukin, V. Klochkov, P. Maksimchuk, V. Seminko, N. Spivak, Oscillations of Cerium Oxidation State Driven by Oxygen Diffusion in Colloidal Nanoceria (CeO_{2-x}), Nanoscale Res. Lett. 12 (2017) 566. doi:10.1186/s11671-017-2339-7.

[45] J. Tauc, A. Menth, States in the gap, J. Non. Cryst. Solids. 8–10 (1972) 569–585. doi:10.1016/0022-3093(72)90194-9.